Coherent optical nonlinearities and phase relaxation of quasi-three-dimensional and quasi-two-dimensional excitons in ZnS_xSe_{1-x}/ZnSe structures

H. P. Wagner,* A. Schätz, and R. Maier
Universität Regensburg, Institut Physik II, D-93040 Regensburg, Germany

W. Langbein and J. M. Hvam
Mikroelectronik Centret, The Technical University of Denmark, Building 345 e, 2800 Lyngby, Denmark
(Received 4 March 1997)

We investigate the dephasing of heavy-hole excitons in different free-standing ZnS_xSe_{1-x}/ZnSe layer structures by spectrally resolved transient four-wave mixing. ZnSe layers of 80, 8, and 4 nm thickness with ternary barriers are studied, representing the crossover from quasi-three-dimensional to quasi-two-dimensional excitons. A common feature of the four-wave-mixing signals is the appearance of two components, a prompt signature and a delayed photon echo, which are identified by their different polarization dependencies and decay times. For crosslinear polarized fields, the rapidly decaying signal is attributed to the response of spin-coupled exciton states, with a decay time given by the inhomogeneous broadening. The photon echo is due to a distribution of localized, noninteracting excitons. We determine the exciton-exciton and exciton-phonon scattering cross sections for different dimensionalities by the intensity and temperature dependencies of the exciton dephasing. [S0163-1829(97)02943-3]

I. INTRODUCTION

The technique of degenerate four-wave mixing (FWM) represents a powerful tool to study fundamental coherent transient phenomena in bulk semiconductors and quantum well (QW) structures. In particular, FWM provides an experimental approach for the investigation of quantum beat phenomena[1–5] and scattering processes of excitons with free carriers,[6–8] excitons,[9–12] and phonons.[10,13–15] The underlying physics is approximately described by the optical Bloch equations.[16–18] The Coulomb interaction and the fermionic nature of the carriers, however, complicate this description so that the use of the semiconductor Bloch equations is generally more appropriate.[19,20] So far these coherent phenomena have been mainly studied in high-quality thin-film III-V layer structures.[1–9,13,14] During the last few years, the epitaxial growth of wide-gap II-VI semiconductors has been improved remarkably due to the world-wide search for blue-green lasers using ZnSe and $Zn_xCd_{1-x}Se$ QW's.[21] Since the wide-gap II-VI materials generally have a higher exciton oscillator strength and a higher third-order nonlinearity[22] than the III-V materials, they are well suited for the study of transient optical phenomena.[10–12,23–27] A comparison of the coherent exciton properties of polar wide-gap II-VI structures with those in III-V structures develops the understanding of the underlying fundamental quasiparticle interaction processes.

In this paper, we report on subpicosecond FWM studies on the heavy-hole excitons (X_h) in free-standing ZnS_xSe_{1-x}/ZnSe layer structures containing ZnSe QW's of different thickness. They cover the range from quasi three-dimensional (3D) to quasi-two-dimensional (2D) excitons with a 2D center-of-mass motion, but a nearly unchanged radius. We investigate the delay-time dependence of the time-integrated (TI) FWM spectra to distinguish the different nonlinear processes contributing. We determine the exciton-exciton and exciton-phonon scattering cross-sections by intensity and temperature dependent measurements of the exciton dephasing rate.

II. EXPERIMENT

All investigated ZnS_xSe_{1-x}/ZnSe layer structures were pseudomorphically grown on (001)-oriented GaAs substrates by low-pressure metal-organic vapor-phase epitaxy (MOVPE). Dimethylzinc-triethylamine, ditertarybutylselenide, and tertary-buthylmercaptan were used in the MOVPE process at a substrate temperature of 340 °C.[28] In three structures, the ZnS_xSe_{1-x} barriers have a sulphur content of 5%, as determined by x-ray diffraction. They enclose ZnSe layers of (number $\times$ thickness) 1×80 nm, covered by 220-nm-thick barriers (sample 80/5), 10×8 nm (sample 8/5), and 10×4 nm (sample 4/5), separated by 40-nm barriers. The fourth structure is like the second, but has a higher barrier sulphur content of 10% (sample 8/10).

In the FWM experiments, a frequency-doubled, mode-locked Ti-sapphire laser was used as excitation source, producing pulses of 100 fs duration and a spectral width of 22 meV at the repetition rate of 76 MHz. The FWM was performed using a degenerate two-pulse configuration in transmission. For this purpose, the GaAs substrate of the samples was removed chemomechanically, producing a free-standing structure adhesively bonded to a sapphire disk. In the density-dependent measurements, we apply a prepulse 20 ps before the first pulse of the self-diffraction experiment arrives on the sample, creating an incoherent background exciton density. The $1/e^2$ focus diameter of all pulses on the sample was measured with a charge-coupled-device camera to 70 μm. The FWM signal was recorded time-integrated and spectrally resolved by a combination of a spectrometer and an optical multichannel analyser as function of the time

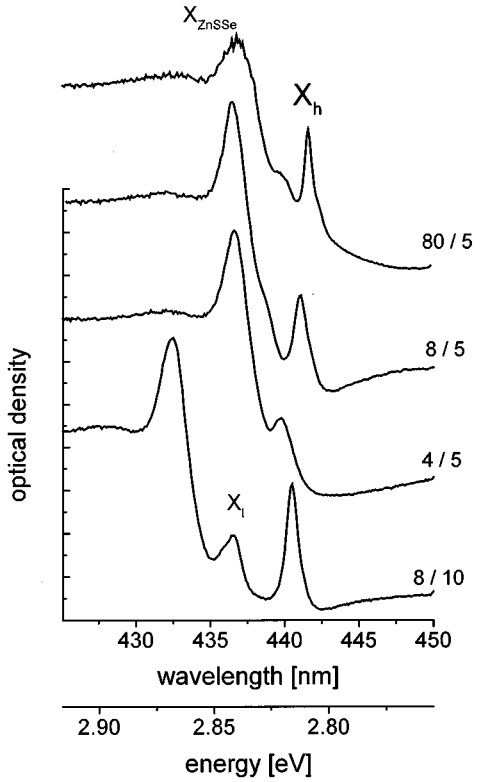

FIG. 1. Absorption spectra of the investigated ZnS_xSe_{1-x}/ZnSe layer structures.

delay τ between the two incident pulses. The sample was kept in a helium bath cryostat allowing temperature dependent measurements. If not otherwise mentioned, the FWM experiments were carried out at a temperature of $T=5$ K.

III. RESULTS AND DISCUSSION

A. Sample characterization

The characterization of the samples is accomplished by transmission, photoreflectance and photoluminescence spectroscopy, x-ray diffraction, and transmission electron microscopy. The absorption spectra of the free-standing layers are summarized in Fig. 1. The dominant absorption line is due to the excitonic transition X_{ZnSSe} of the ZnS_xSe_{1-x} barriers followed by their interband continuum at higher energies. Around $\lambda=442$ nm, the heavy-hole exciton X_h of the ZnSe QW's appears, shifting to higher energies with decreasing well width due to the increasing hole confinement energy. In sample 8/10, the light-hole exciton transition (X_l), which is strain and confinement split from the X_h, is resolved at $\lambda=437.5$ nm, while it merges with the barrier transition X_{ZnSSe} in samples 8/5 and 4/5. The optical density of the X_h transitions and their intensity full width at half maximum (FWHM) linewidth ΔE are determined by fitting the observed absorption spectra with a theoretical exciton absorption model.[29,30] The energetic positions of the X_h transitions, their optical densities and linewidths are summarized in Table I for all samples investigated.

Photoluminescence spectra of the samples reveal a distinct donor-bound exciton transition I_2 caused by chlorine atoms, which are introduced as impurities from the ditertarybutylselenide precursor.[31] The Cl donors are 90% compensated and reach a concentration of $\approx 10^{16}$ cm^{-3} in bulk ZnSe layers.[32]

TABLE I. Energetic positions of the X_h exciton transition E_X and corresponding optical densities OD and intensity FWHM linewidths ΔE of the investigated ZnS_xSe_{1-x}/ZnSe structures.

Structure	E_X (eV)	OD	ΔE (meV)
80 nm/5%	2.8068	1.3	3.9
8 nm/5%	2.8105	0.9	6.4
4 nm/5%	2.8183	0.7	7
8 nm/10%	2.8138	1.4	5.1

Photoreflectance measurements have shown, that the conduction-band offset in ZnS_xSe_{1-x}/ZnSe structures pseudomorphically grown on GaAs is less than 2 meV (Ref. 33) for $x<0.15$. Consequently, only the holes are confined in the ZnSe QW's, resulting in strain and confinement split X_h and X_l excitons with nearly bulk exciton binding energies of $E_{bX}=20$ meV and an exciton Bohr radius of $a_x=4.3$ nm, even for QW widths comparable to a_x.

The important structural defects which limit the crystal quality of our samples are stacking faults due to Shockley-type partial dislocations, which are found at a layer thickness of $d>130$ nm in transmission electron microscopy investigations.[34,35] The density of these partial dislocations increases up to the critical thickness of the ZnS_xSe_{1-x}/GaAs system, which is depending on the sulphur content (lattice matching is reached at a sulphur concentration of $x\approx 0.07$). Above the critical thickness, full dislocations are generated, leading to strain relaxation in the ZnS_xSe_{1-x} layer. All structures investigated here are well below this thickness. However, the $ZnS_{0.05}Se_{0.95}$/ZnSe samples are closer to it than sample 8/10, and thus a lower amount of stacking faults is expected in the latter structure, which is supported by x-ray measurements.[36]

B. FWM signal analysis

Based on the solution of the optical Bloch equations for a two-level system, it is known that the emitted FWM signal in the $2\mathbf{k}_2-\mathbf{k}_1$ direction of a single, homogeneously broadened transition is a free polarization decay (FPD), starting in real time with the arrival of the probe pulse $\mathbf{k}_2$. If the system is inhomogeneously broadened, the FPD of the different transitions destructively interfere, the prompt coherent emission is suppressed, and a photon echo (PE) is emitted a delay time τ after the probe pulse, with a duration given by the inhomogeneous broadening. The TI FWM involving a PE shows a maximum at a finite positive delay time τ between pump and probe pulse, in contrast to the maximum at zero delay time for a FPD. For purely homogeneously (inhomogeneously) broadened two-level systems, the dephasing time T_2 is given by the exponential decay $I_{\mathrm{FWM}}(\tau)\propto I(0)e^{-c\tau/T_2}$ of the TI FWM signal for $\tau\gg T_2$, where $c=2$ ($c=4$).

In all investigated samples, a fast and pronounced initial decrease of the FWM signal and a delayed PE is observed in the TI FWM traces, as shown in Fig. 2. The excitation energy was centered below the X_h transition in order to avoid

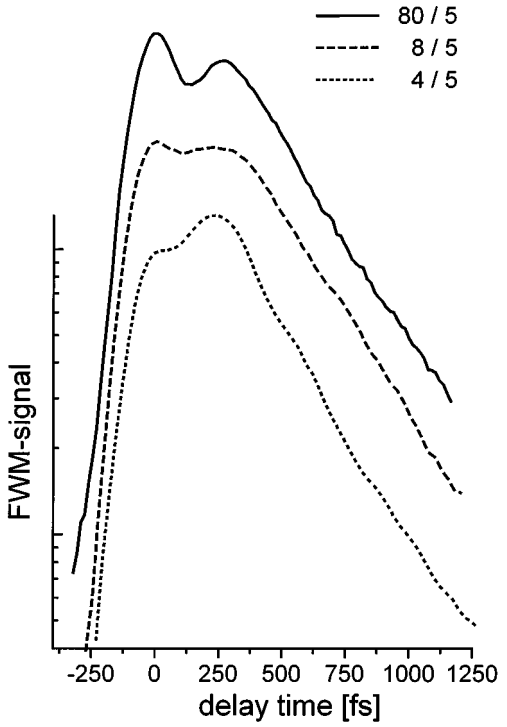

FIG. 2. TI FWM signals vs delay time at the X_h energetic position in the $ZnS_{0.05}Se_{0.95}$ samples for low excitation densities and $T=10$ K.

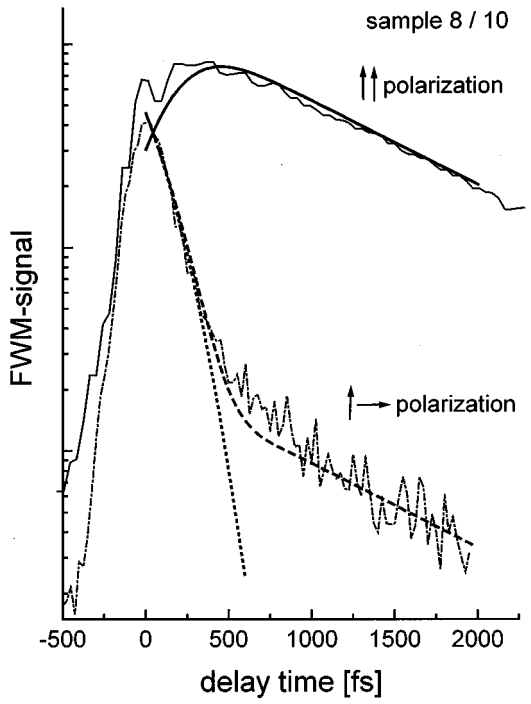

FIG. 3. TI FWM signal vs delay time obtained at the X_h transition energy of sample 8/10 for different polarized fields as labeled. The thick full and thick dotted curves are calculated FWM traces for $(\uparrow,\uparrow)$ and $(\uparrow,\rightarrow)$ polarization according to Eq. (1). The thick dashed curve is calculated using an angle of $\theta_{12}=86°$ between the polarizations.

contributions of higher transitions such as the X_h continuum or the X_l. For a better discrimination of the two components, polarization-dependent measurements were performed on sample 8/10, shown in Fig. 3. Going from collinear $(\uparrow,\uparrow)$ to crosslinear $(\uparrow,\rightarrow)$ polarized excitation pulses, the PE component drastically decreases (by a factor of 25), while the prompt component is only reduced by a factor of 2. Cocircular polarization (σ^+,σ^+) results in a similar FWM signal (not shown here) as in the $(\uparrow,\uparrow)$ configuration. For crosscircular polarized pulses (σ^+,σ^-), both FWM components are suppressed by a factor of 10 compared to the (σ^+,σ^+) configuration. Figure 4 shows the spectrally resolved FWM signals at zero and 1 ps delay for $(\uparrow,\uparrow)$, $(\uparrow,\rightarrow)$, and (σ^+,σ^+) polarized excitation. The spectra at zero delay, which are dominated by the prompt contribution, have a linewidth of 5 meV, equal to the absorption linewidth. They show a small dip at the X_h energy due to reabsorption. For different polarizations, a slight energetic shift is observed due to different strength of biexcitonic contributions. The biexciton induced signal is resolved for 1 ps delay [Fig. 4(b)] as a low-energy peak, which disappears in the (σ^+,σ^+) configuration and gains relative intensity in the $(\uparrow,\rightarrow)$ configuration. The involved transition from a biexciton (XX) to an exciton (X_h) reveal a biexciton binding energy of $E_{bXX}=5.5\pm0.5$ meV. The biexcitonic nature is supported by quantum beats with the expected period of $T_{\mathbf{beat}}=750$ fs in the FWM traces at the XX energy for $(\uparrow,\uparrow)$ and $(\uparrow,\rightarrow)$ polarization, showing a phase shift in agreement to similar investigations in GaAs QWs.[4] The PE spectrum is redshifted by 2 meV from the X_h absorption, in agreement with its assignment to localized, noninteracting excitons. The presence of the signal in (σ^+,σ^-) configuration indicates a coupling of σ^+ and σ^- excitons, presumably by the disorder. Assuming a Gaussian distribution function $g(J)$ of the coupling strength J, the third-order nonlinear polarization vector in the component parallel and orthogonal to the polarization of the pump pulse reads[3]

$$\vec{P}^{\,(3)}_{2\vec{k}_1-\vec{k}_2}(t,\tau)\propto\Theta(t-\tau)\Theta(\tau)e^{-i\Omega_h(t-\tau)} \times e^{i\Omega_h^*\tau}\begin{bmatrix}\cos(\theta_{12})g(t-2\tau)\\ -\sin(\theta_{12})g(t)\end{bmatrix}, \qquad (1)$$

where the complex frequency $\Omega_h=\omega_h-i\gamma_h$ contains the exciton transition energy ω_h and dephasing rate $\gamma_h=1/T_2$, θ_{12} is the angle between the linear polarizations of pulse 1 and pulse 2, $\Theta(t)$ is the Heavyside function, and $g(t)$ is the Fourier transform of $g(J)$. Figure 3 shows the calculated TI-FWM traces at the X_h transition obtained from the Fourier-transformed Eq. (1) for the $(\uparrow,\uparrow)$ and $(\uparrow,\rightarrow)$ polarization configuration. The parameters $T_2=4.2$ ps and a linewidth of $\Delta E=3.5$ meV are determined from the FWM spectrum at $\tau=1$ ps. A photon echo is obtained in the $(\uparrow,\uparrow)$ configuration, $\theta_{12}=0$ (thick drawn line in Fig. 3), while in the $(\uparrow,\rightarrow)$ configuration $\theta_{12}=\pi$, the signal shows a fast decay (dotted line), determined by $g(t)$. An agreement with the experimentally observed FWM signal is achieved (thick dotted line) at an angle of $\theta_{12}=86°$, which might be due to an limited experimental polarization purity of the half-wave plate used. The predicted FWM spectra, also displayed in Fig. 4, are, besides the already discussed biexcitonic contribution, in reasonable agreement with the experiment. The

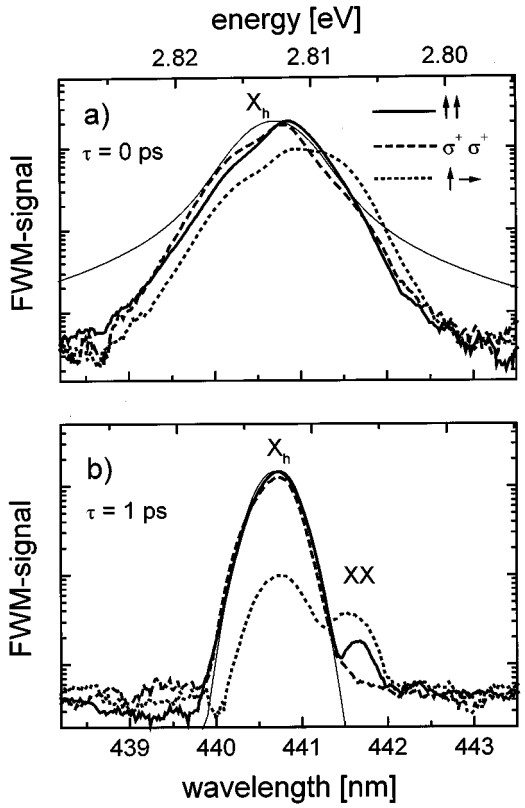

FIG. 4. TI FWM spectra excited resonantly to the X_h in sample 8/10 for $(\uparrow,\uparrow)$, $(\uparrow,\rightarrow)$, and (σ^+,σ^+) polarization at a delay time of (a) 0 ps and (b) 1 ps. The thin full lines show the corresponding calculated spectra obtained from the optical Bloch equations.

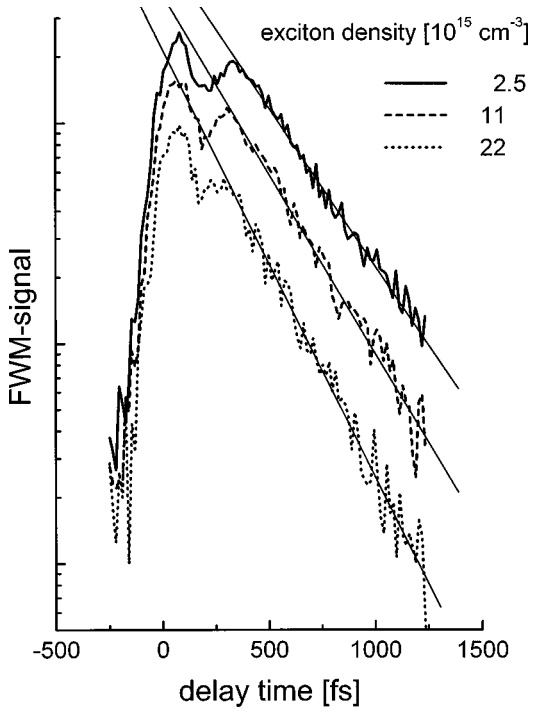

FIG. 5. TI FWM traces at the X_h energy in sample 80/5 at various incoherent exciton densities, as given.

calculated stronger broadening at zero delay is due to the assumed markovian dephasing, which is erroneous for short times (large energies).

Various models have been proposed recently to describe the appearance of a prompt signal found in similar investigations on GaAs QW structures. It was shown by time-resolved FWM measurements, that low-intensity $(\uparrow,\uparrow)$ and $(\uparrow,\rightarrow)$ polarized excitation gives rise to a PE and to a prompt signal or FPD, respectively.[37–40] Since the delayed signal saturates at smaller intensities than the FPD a two-component behavior has been observed under appropriate conditions similar to our observations. These results were attributed to the coexistence of extended and localized excitons due to interface fluctuations in the QW giving rise to a FPD and PE signals, respectively. Another investigation[41] exposed a deviation of the PE behavior but no clear FPD signal in the time-resolved FWM measurements that were carried out in $(\uparrow,\uparrow)$ configuration. Corresponding TI FWM, however, reveals a fast initial decay similar to our observations, which can be modeled by the simultaneous influence of disorder and Coulomb interactions. Furthermore combinations of other exciton-exciton interaction effects as excitation induced dephasing[42] and biexciton formation,[43,44] as well as the influence of intersite disorder[45] also can lead to a two-component behavior under certain conditions.

Since all our measurements are based on time integrated FWM experiments it is difficult to conclude which of the effects are dominating the prompt signature in the $(\uparrow,\uparrow)$ configuration. Due to the fast decay, it is more likely that exciton-exciton interaction effects are responsible for the observed behavior[41–44] than a FPD of extended excitons proposed by Refs. 37–40. Future time-resolved measurements will provide more information about the complex nature of the two-component behavior in the FWM spectra.

C. Exciton-exciton scattering

In order to investigate the exciton scattering rate with incoherent excitons, intensity dependent measurements were performed. For this purpose, an incoherent background density of X_h excitons is created by a prepump pulse applied 20 ps before the first FWM pulse. The average prepump exciton density n_X in the quasi-3D sample was determined using the relation

$$n_X=\frac{N_{hv}(1-e^{(-\mathrm{OD})})w(1-R)}{\pi a^2 d}. \tag{2}$$

Here N_{hv} is the total number of photons of the prepump pulse, w is the ratio of the X_h absorption linewidth to the spectral width of the laser pulse, and R accounts for reflection losses. OD is the peak optical density of the X_h transition, d is the ZnSe layer thickness and a is the $1/e^2$ focus diameter of the pulses on the sample.

Figure 5 shows the intensity dependent FWM in the $(\uparrow,\uparrow)$ configuration on sample 80/5, using an excitation centered below the X_h transition. With increasing exciton density, the FWM intensity decreases, which is attributed to the bleaching of the X_h. Furthermore, the delay of the PE maximum is reduced, since the ratio between inhomogeneous to homoge-

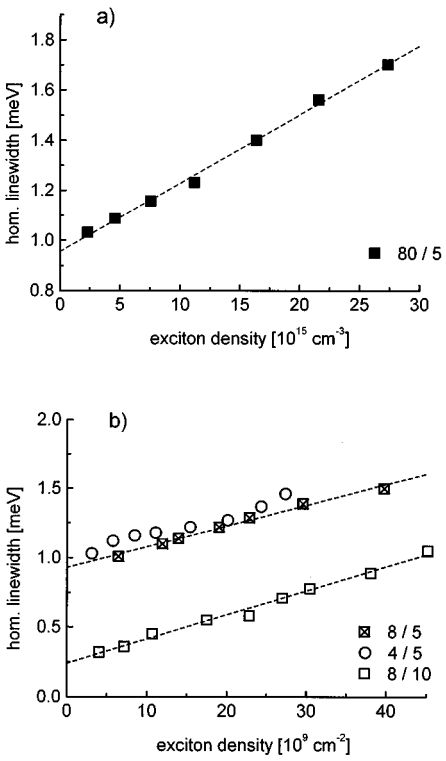

FIG. 6. Homogeneous linewidth as a function of the incoherent exciton density for the (a) quasi-3D exciton system and (b) quasi-2D exciton systems. The dashed curves are fits according to Eq. (3).

neous broadening $r=\Gamma_{Xh}/\gamma_{Xh}$ decreases. However, it remains larger than six even for the highest excitation densities used. The extracted homogeneous linewidths $\gamma_{\mathrm{hom}}=h/(\pi T_2)$ are plotted in Fig. 6(a) as a function of the exciton density. The linear increase of γ_{hom} is due to an exciton-exciton collision broadening,[46,47] which can be described by

$$\gamma_{\mathrm{hom}}(n_X)=\gamma_{\mathrm{hom}}(0)+\beta_{XX}^{(m\mathrm{D})}a_B^{*m}E_B n_x. \tag{3}$$

Here, a_B^* is the exciton Bohr radius, E_B is the exciton binding energy, m is the dimensionality ($m=3$ for bulk crystals), and $\beta_{XX}^{(m\mathrm{D})}$ is a dimensionless exciton-exciton scattering parameter. The homogeneous line width $\gamma_{\mathrm{hom}}(0)$ is extrapolated to 0.9 meV in this sample. It includes all residual intrinsic and extrinsic interactions of excitons with phonons, stacking faults, interfaces, and impurities at a temperature of $T=10$ K. The value of the interaction parameter $\beta_{XX}^{(3\mathrm{D})}$ is fitted to 19 ± 8, where the error is given mainly by the systematic experimental uncertainty of the exciton density.

Also for the quasi-2D structures, a linear density dependence of the determined homogeneous widths is observed [Fig. 6(b)]. It is fitted by Eq. (3), with the two-dimensional interaction parameter $\beta_{XX}^{(2\mathrm{D})}$. The mean exciton densities per QW are determined according to Eq. (2), where the excitation volume $V=\pi a^2 d$ is substituted by the excitation area $A=\pi a^2$ multiplied by the number of QW's present. It is conspicuous that the background homogeneous width $\gamma_{\mathrm{hom}}(n_X=0)\approx0.9$ meV of all $ZnS_{0.05}Se_{0.95}$ samples is about three times larger than in the $ZnS_{0.1}Se_{0.9}$ sample 8/10. We attribute this to the higher concentration of stacking faults in the $ZnS_{0.05}Se_{0.95}$ structures. As expected, the exciton-exciton scattering parameter, which has a value of $\beta_{XX}^{(2\mathrm{D})}\approx5$ for all QW samples, is not affected by their structural quality.

TABLE II. Exciton-exciton collision parameters $\beta_{XX}^{(m\mathrm{D})}$, exciton-acoustic and exciton-optical phonon scattering parameters β_{ac},β_{LO}, and background homogeneous linewidths $\gamma_{\mathrm{hom}}(0)$ of all investigated samples.

Structure	$\beta_{XX}^{(m\mathrm{D})}$	β_{ac} (μeV/K)	β_{LO} (meV)	$\gamma_{\mathrm{hom}}(0)$ (meV)
80 nm/5%	19±6	9.5±1.5	75±21	0.85
8 nm/5%	5±1.6	10.2±1.5	114±13	0.8
4 nm/5%	5.1±1.7	15.2±1	118±15	0.75
8 nm/10%	4.7±1.5	7.5±1	87±7	0.2

All determined exciton-exciton scattering parameters are summarized in Table II. The values are in agreement with previous measurements using a two-beam configuration if the inhomogeneous broadening is considered.[11,24] They are somewhat larger than values found in bulk GaAs and GaAs QW's,[6,13] but are by more than one order of magnitude larger than values obtained in $CdTe/Cd_xMn_{1-x}Te$ QW's (Ref. 10) and $Zn_xCd_{1-x}Se/ZnSe$ QW's.[12]

A comparison of the collision broadening $\Delta\Gamma=\gamma_{\mathrm{hom}}(n_X)-\gamma_{\mathrm{hom}}(0)$ in the quasi-3D and quasi-2D exciton systems is available using the exciton-exciton distance in units of the exciton Bohr radius a_B^* instead of the excitation density,[13] shown in Fig. 7. In these units, the exciton-exciton scattering is stronger for the quasi-2D excitons as compared with the quasi-3D excitons. This is explained by the reduced phase space in a 2D system, causing an increased repulsive interaction between excitons due to the Pauli blocking.

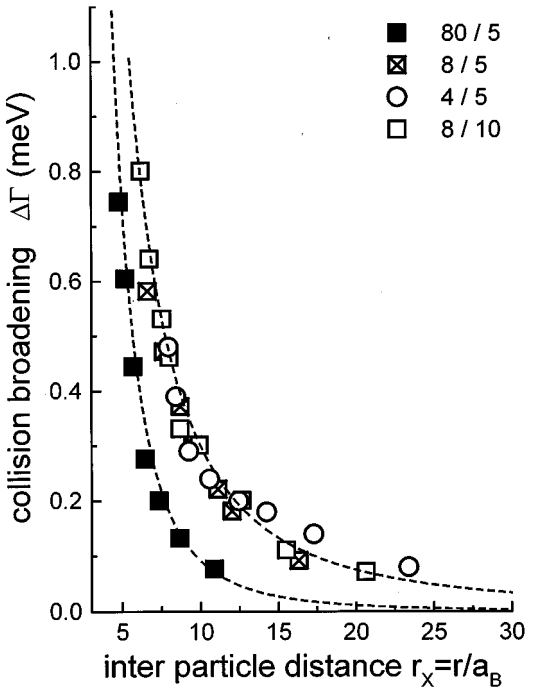

FIG. 7. Exciton-exciton collision broadening for quasi-3D and quasi-2D X_h excitons vs the normalized exciton-exciton distance r_X. The dashed curves are fits according to Eq. (3).

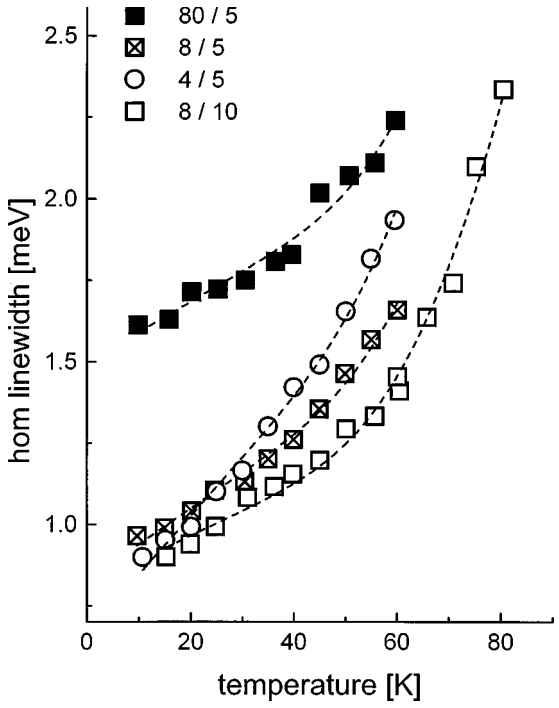

FIG. 8. Homogeneous linewidth of the X_h excitons versus the lattice temperature for the different samples as labeled. The dashed curves are fits according to Eq. (4).

D. Exciton-phonon scattering

Since the density of acoustic and optical phonons increases with increasing temperature, the temperature dependence of the homogeneous linewidth can be used to determine the exciton-phonon scattering strength. In deriving the homogeneous line width $\gamma_{\mathrm{hom}}(T,n_X)$ as a function of temperature from the FWM decay, a strongly inhomogeneously broadened exciton system is assumed, which is valid in the considered temperature range. Figure 8 shows the resulting linewidth for all investigated samples. Its temperature dependence exhibits two different temperature regimes. At temperatures below 40 K, the linewidth is increasing linearly with increasing temperature due to the acoustic-phonon exciton interaction. At higher temperatures, the slope increases, indicating the onset of the optical-phonon scattering. The larger homogeneous linewidth in sample 80/5 compared to other samples is due to a higher excitation intensity used in the measurements. The temperature dependence is fitted using the acoustic phonon scattering parameter β_{ac} and the optical-phonon scattering parameter β_{LO} according to the following relation expected in first-order perturbation theory:[48,49]

$$\gamma_{\mathrm{hom}}(T,n_x)=\gamma_{\mathrm{hom}}(0,n_x)+\beta_{\mathrm{ac}}T+\frac{\beta_{\mathrm{LO}}}{\exp(E_{\mathrm{LO}}/k_BT)-1}. \tag{4}$$

Here, $E_{\mathrm{LO}}=31.6$ meV is the longitudinal-optical-phonon energy, k_B is the Boltzmann constant, and $\gamma_{\mathrm{hom}}(0,n_X)$ contains the low-temperature homogeneous linewidth described in the last section. A temperature-dependent scattering of excitons at ionized impurities was not taken into account, since the increase of thermally created ionized chlorine donors is small compared to the background ionized-impurity concentration, due to the high compensation ratio. The obtained values of β_{ac} and β_{LO} are collected in Table II.

The results show that the interaction strength of optical phonons with quasi-2D excitons of the $ZnS_{0.05}Se_{0.95}$ samples is somewhat larger compared to the interaction with bulk excitons. In sample 8/10, β_{LO} is found close to the value of the quasi-3D system. In all samples the optical-phonon energy $\hbar\omega_{\mathrm{LO}}$ exceeds the exciton binding energy $E_{bX}\approx 20$ meV. Therefore, after the phonon absorption, the exciton is either ionized, or the energy is transferred into center-of-mass energy (intraband contribution). The nearly constant ratio of the exciton binding energy to the LO phonon energy $E_{bX}/\hbar\omega_{\mathrm{LO}}$ should lead to comparable exciton ionization rates in all samples. Therefore, the similarity of the scattering parameter β_{LO} in samples 80/5 and 8/10 indicates that the cross section due to intraband scattering is either small, as mentioned in Ref. 50, or similar for quasi-3D or quasi-2D excitons. In the $ZnS_{0.05}Se_{0.95}$ samples, $\hbar\omega_{\mathrm{LO}}$ also exceeds the hole ionization energy to the barrier, so that the confined exciton can be scattered into the barrier. This additional scattering channel might explain the slightly higher optical-phonon scattering parameters β_{LO} in these structures. The observed $\beta_{\mathrm{LO}}\approx 90$ meV clearly exceeds the value of 10 meV obtained in GaAs QW's,[14] which is due to the higher polarity of the II–VI material compared to the III–V compounds.

The acoustic-phonon exciton interaction β_{ac} shows an increase from about 8 μeV/K in samples 80/5, 8/10, and 8/5 to 15 μeV/K in the sample 4/5. This increase is attributed to an increasing deformation-potential scattering with decreasing well width.[51] The value of β_{ac} in the bulk sample 80/5 exceeds that in GaAs by a factor of 2, due to the higher deformation-potential interaction in ZnSe.[48] The observed scattering parameters are in agreement with those obtained in bulk ZnSe and $Zn_xCd_{1-x}Se$/ZnSe QW's (Ref. 12) and CdTe QW's.[10]

Finally, the extrapolated background homogeneous linewidth $\gamma_{\mathrm{hom}}(0)=\gamma_{\mathrm{hom}}$ ($T=0$ K, $n_X=0$) gives us a measure of the structural quality. In all investigated samples, it is higher than reported for GaAs QW (Refs. 6 and 13) indicating a lower structural quality. This is in agreement with the higher dislocation density and the high ionized-impurity concentration in the samples.

IV. SUMMARY

We have performed transient FWM at low temperatures to study the dephasing of heavy-hole excitons in pseudomorphically grown ZnS_xSe_{1-x}/ZnSe/GaAs structures containing ZnSe QW's of different thickness. The TI FWM indicates the simultaneous appearance of a pronounced prompt signature and a delayed photon echo, showing different polarization dependencies and dephasing times. The rapid decay in $(\uparrow,\rightarrow)$ polarized excitation is attributed to disorder induced coupling of free excitons of different spin. The photon echo signal is generated by the inhomogeneous distribution of localized, noninteracting excitons.

Density-dependent measurements yield exciton-exciton interaction strengths that are comparable to those obtained in GaAs structures. This implies that the FWM signal obtained from II-VI QW structures is strongly affected

by excitation-induced dephasing.

The deduced acoustic phonon exciton interaction parameter is two times higher compared to GaAs QW's, due to the higher deformation potential in ZnSe. The optical phonon-exciton interaction parameter is found to be strongly enhanced compared to the less polar III-V semiconductors due to the stronger Fröhlich interaction in the II-VI material ZnSe.

ACKNOWLEDGMENTS

The experimental support of K. Litvinenko and V. Mizeikis is kindly acknowledged. We thank B. Hahn and W. Gebhardt for providing the ZnS_xSe_{1-x}/ZnSe structures. This work is supported by the Deutsche Forschungsgemeinschaft and by the Danish Ministries of Research and Education in the framework of the Centre for Nanostructures.

*Author to whom correspondence should be addressed. Fax: ++49 9419434226. Electronic address: Hans-Peter.Wagner@physik.uni-regensburg.de

[1] E. O. Göbel, K. Leo, T. C. Damen, J. Shah, S. Schmitt-Rink, W. Schäfer, J. F. Müller, and K. Köhler, Phys. Rev. Lett. **64**, 792 (1990).

[2] K. Leo, T. C. Damen, J. Shah, and K. Köhler, Phys. Rev. B **42**, 11 359 (1990).

[3] D. Bennhardt, P. Thomas, R. Eccleston, K. J. Mayer, and J. Kuhl, Phys. Rev. B **47**, 13 485 (1993).

[4] E. J. Mayer, G. O. Smith, V. Heuckeroth, J. Kuhl, K. Bott, A. Schulze, T. Meier, S. W. Koch, and P. Thomas, R. Hey and K. Ploog, Phys. Rev. B **51**, 10 909 (1995).

[5] J. Erland, D. Birkedal, V. G. Lyssenko, and J. M. Hvam, J. Opt. Soc. Am. B **13**, 981 (1996).

[6] L. Schultheis, J. Kuhl, A. Honold, and C. W. Tu, Phys. Rev. Lett. **57**, 1635 (1986).

[7] J.-Y. Bigot, M. T. Portella, R. W. Schönlein, and C. V. Shank, Phys. Rev. Lett. **67**, 636 (1991).

[8] D.-S. Kim, J. Shah, J. E. Cunningham, T. C. Damen, S. Schmitt-Rink, and W. Schäfer, Phys. Rev. Lett. **68**, 2838 (1992).

[9] A. Honold, L. Schultheis, J. Kuhl, and C. W. Tu, Phys. Rev. B **40**, 6442 (1989).

[10] R. Hellmann, M. Koch, J. Feldmann, S. T. Cundiff, E. O. Göbel, D. R. Yakovlev, A. Waag, and G. Landwehr, J. Cryst. Growth **138**, 791 (1994).

[11] H. P. Wagner, J. Lehmann, and B. Hahn, J. Lumin. **66&67**, 84 (1996).

[12] A. J. Fischer, D. S. Kim, J. Hays, W. Sham, J. J. Song, D. B. Eason, J. Ren, J. F. Schetzina, H. Luo, and J. K. Furdyna, Phys. Rev. B **50**, 17 643 (1994).

[13] L. Schultheis, A. Honold, J. Kuhn, J. Köhler, and C. W. Tu, Phys. Rev. B **34**, 9027 (1986).

[14] D. S. Kim, J. Shah, J. E. Cunningham, T. C. Damen, W. Schäfer, M. Hartmann, and S. Schmitt-Rink, Phys. Rev. Lett. **68**, 1006 (1992).

[15] A. J. Fischer, D. S. Kim, J. Hays, W. Shan, J. J. Song, D. B. Eason, J. Ren, J. F. Schetzina, H. Luo, J. K. Furdyna, Z. Q. Zhu, T. Yao, J. F. Kiem, and W. Schäfer, Phys. Rev. Lett. **73**, 2368 (1994).

[16] T. Yajima and Y. Taira, J. Phys. Soc. Jpn. **47**, 1620 (1979).

[17] J. Erland and I. Baslev, Phys. Rev. A **48**, R1765 (1993).

[18] J. Erland, K.-H. Pantke, V. Mizeikis, V. G. Lyssenko, and J. M. Hvam, Phys. Rev. B **50**, 15 047 (1994).

[19] M. Lindberg, and S. W. Koch, Phys. Rev. B **38**, 3342 (1988).

[20] M. Wegener, D. S. Chemla, S. Schmitt-Rink, and W. Schäfer, Phys. Rev. A **42**, 5675 (1990).

[21] M. A. Haase, J. Qiu, J. M. DePuydt, and H. Cheng, Appl. Phys. Lett. **59**, 1272 (1991).

[22] T. Saiki, K. Takeuchi, and M. Kuwata-Gonokamie, Appl. Phys. Lett. **60**, 192 (1992).

[23] D. Weckendrup, M. Saschek, U. Neukirch, J. Gutowski, S. O. Ferreira, and H. Sitter, J. Appl. Phys. **77**, 4145 (1996).

[24] H. P. Wagner, J. Lehmann, and B. Hahn, Solid-State Electron. **40**, 745 (1996).

[25] T. Häupl, H. Nickolaus, F. Henneberger, and A. Schülzgen, Phys. Status Solidi B **194**, 219 (1996).

[26] U. Neukirch, D. Weckendrup, K. Wundke, J. Gutowski, and D. Hommel, J. Opt. Soc. Am. B **13**, 1256 (1996).

[27] H. Nickolaus, F. Henneberger, and A. Schülzgen, J. Cryst. Growth **159**, 780 (1996).

[28] H. Stanzl, T. Reisinger, K. Wolf, M. Kastner, B. Hahn, and W. Gebhardt, Phys. Status Solidi B **187**, 303 (1995).

[29] Y. Toyozawa, Prog. Theor. Phys. **27**, 89 (1962).

[30] A. R. Goni, A. Canterero, K. Syassen, and M. Cardona, Phys. Rev. B **41**, 10 111 (1990).

[31] K. Wolf, A. Elstner, H. Stanzl, T. Reisinger, and W. Gebhardt, J. Lumin. **65**, 185 (1995).

[32] B. Hahn (private communication).

[33] S. Lankes, T. Reisinger, B. Hahn, C. Meier, M. Meier, and W. Gebhardt, J. Cryst. Growth **159**, 480 (1996).

[34] A. Rosenauer, T. Reisinger, F. Franzen, G. Schötz, B. Hahn, K. Wolf, J. Zweck, and W. Gebhardt, J. Appl. Phys. **79**, 4124 (1996).

[35] A. Rosenauer, H. Preis, M. Kastner, B. Hahn, and W. Gebhardt (unpublished).

[36] M. J. Kastner, G. Leo, C. Auchter, B. Hahn, and W. Gebhardt, Cryst. Res. Technol. **31**, 789 (1996).

[37] M. D. Webb, S. T. Cundiff, and D. G. Steel, Phys. Rev. B **43**, 12 658 (1991).

[38] M. D. Webb, S. T. Cundiff, and D. G. Steel, Phys. Rev. Lett. **66**, 934 (1991).

[39] S. T. Cundiff and D. G. Steel, IEEE J. Quantum Electron. **28**, 2423 (1992).

[40] S. T. Cundiff, H. Wang, and D. G. Steel, Phys. Rev. B **46**, 7248 (1992).

[41] F. Jahnke, M. Koch, T. Meier, J. Feldmann, W. Schäfer, P. Thomas, S. W. Koch, E. O. Göbel, and H. Nickel, Phys. Rev. B **50**, 8114 (1994).

[42] Y. Z. Hu, R. Binder, S. W. Koch, S. T. Cundiff, H. Wang, and D. G. Steel, Phys. Rev. B **49**, 14 382 (1996).

[43] A. E. Paul, J. A. Bolger, A. L. Smirl, and J. G. Pellegrino, J. Opt. Soc. Am. B **13**, 1016 (1996).

[44] J. A. Bolger, A. E. Paul, and A. L. Smirl, Phys. Rev. B **16**, 11 666 (1996).

[45] Ch. Lonsky, P. Thomas, and A. Weller, Phys. Rev. Lett. **63**, 652 (1989).

[46] F. Boldt, K. Henneberger, and V. May, Phys. Status Solidi B **130**, 675 (1985).

[47] G. Manzke, K. Henneberger, and V. May, Phys. Status Solidi B **139**, 233 (1987).

[48] S. Rudin, T. L. Reinecke, and B. Segall, Phys. Rev. B **42**, 11 218 (1990).
[49] S. Rudin and T. L. Reinecke, Phys. Rev. B **41**, 3017 (1990).
[50] N. T. Pelekanos, J. Ding, M. Hagerott, A. V. Nurmikko, H. Luo, N. Samarth, and J. K. Furdyna, Phys. Rev. B **45**, 6037 (1992).
[51] J. Lee, E. S. Koteles, and M. O. Vassell *et al.*, Phys. Rev. B **33**, 5512 (1986).